

Low-Ionization Outflows in High Eddington Ratio Quasars

Paola Marziani¹, Jack W. Sulentic, Ilse Plauchu-Frayn, Ascensión del Olmo

Instituto de Astrofísica de Andalucía, CSIC, Granada, Spain

ABSTRACT

The broad MgII λ 2800 doublet has been much studied in connection with its potentially important role as a virial estimator of black hole mass in high redshift quasars. An important task is therefore identification of any line components likely related to broadening by non-virial motions. High s/n median composite spectra (binned in the “4D eigenvector 1” context of Sulentic et al. 2007) were constructed for the brightest 680 SDSS DR7 quasars in the $0.4 \leq z \leq 0.75$ range where both MgII λ 2800 and H β are recorded in the same spectra. Composite spectra representing 90% of the quasars confirm previous findings that FWHM(MgII λ 2800) is about 20% narrower than FWHM(H β). The situation is clearly different for the most extreme (Population A) sources which are the highest Eddington radiators in the sample. In the median spectra of these sources FWHM MgII λ 2800 is equal to or greater than FWHM(H β) and shows a significant blueshift relative to H β . We interpret the MgII λ 2800 blueshift as the signature of a radiation-driven wind or outflow in the highest accreting quasars. In this interpretation the MgII λ 2800 line width – affected by blueshifted emission – is unsuitable for virial mass estimation in $\approx 10\%$ of quasars.

Subject headings: quasars: general — quasars: emission lines — quasars: individual (SDSS J150813.02+484710.6)

1. Introduction

Estimation of black hole mass (M_{BH}) and Eddington ratio (L/L_{Edd}) for quasars is of great interest both to researchers working on models of the broad line region (BLR) structure and to cosmologists. Therefore we need a large number of accurate as possible estimates over the widest possible range of redshift, source luminosity and line/continuum properties. FWHM(H β) is the principal virial estimator at low redshifts. While H β can be followed into

¹INAF, Astronomical Observatory of Padova, Padova, Italy. e-mail paola.marziani@oapd.inaf.it

the infrared (out to $z \approx 3.7$) at least one additional line is needed to provide complementary M_{BH} estimates over the full redshift range where quasars are observed. $\text{MgII}\lambda 2800$ is the best candidate since it is a low-ionization line and avoids some of the difficulties associated with $\text{CIV}\lambda 1549$ (e.g. Netzer et al. 2007; Sulentic et al. 2007; Marziani & Sulentic 2012; Trakhtenbrot & Netzer 2012; Denney 2012).

The advent of the SDSS database makes possible a direct calibration of $\text{MgII}\lambda 2800$ using sources where *both* $\text{MgII}\lambda 2800$ and $\text{H}\beta$ appear in the same SDSS spectra. Only high s/n composite spectra can provide an ideal vehicle for such comparisons. In addition one has to consider that source diversity found within the context of a formalism like 4D Eigenvector 1 (4DE1 Sulentic et al. 2000, 2007; Marziani et al. 2010) is large and likely driven by Eddington ratio L/L_{Edd} (e.g. Boroson & Green 1992; Marziani et al. 2001; Boroson 2002; Grupe 2004; Kruczek et al. 2011; Tang et al. 2012). The 4DE1 allows to discriminate sources whose emission line profiles and whose spectrophotometric properties are strikingly different. A notable empirically-motivated boundary at low- and moderate luminosity is set by $\text{FWHM}(\text{H}\beta) \approx 4000 \text{ km s}^{-1}$. Sources narrower than this limit show $\text{H}\beta$ profiles that are well fit by a Lorentzian function, while broader sources show prominent redward asymmetries in their $\text{H}\beta$ profiles (e.g. Véron-Cetty et al. 2001; Marziani et al. 2003b). Sources with $\text{FWHM}(\text{H}\beta) \leq 4000 \text{ km s}^{-1}$ include Narrow Line Seyfert 1s (NLSy1s) by definition and are characterized by a significant high-ionization outflow, revealed by a $\text{CIV}\lambda 1549$ blueshift with respect to rest frame or to broad low-ionization lines (e.g. Gaskell 1982; Tytler & Fan 1992; Marziani et al. 1996; Sulentic et al. 2007; Richards et al. 2011). The outflow has been ascribed to a radiative or magnetically driven wind (e.g. Murray & Chiang 1997; Bottorff et al. 1997; Proga et al. 2000). Therefore it is important to at least distinguish between sources that appear to be wind- or disk-dominated (Richards et al. 2011) applying the limit at $\text{FWHM}(\text{H}\beta) = 4000 \text{ km s}^{-1}$ that separates Population A and B sources (Sulentic et al. 2000, c.f. Collin et al. 2006).

A finer subdivision is still needed even with the restriction to Population A. Pop. A sources span a relatively large range in Eddington ratio, $\Delta \log L/L_{\text{Edd}} \approx 0.5$, that likely involves not only the highest Eddington radiators. We apply the spectral classification of Sulentic et al. (2002) that divides the plane $\text{FWHM}(\text{H}\beta) - R_{\text{FeII}}$ into bins of $\Delta R_{\text{FeII}} = 0.5$ and $\Delta \text{FWHM}(\text{H}\beta) = 4000 \text{ km s}^{-1}$, where R_{FeII} is computed as the equivalent width (or intensity) ratio of the $\text{FeII}\lambda 4570$ blend and broad $\text{H}\beta$ (see their Fig. 1). Extreme Pop. A (A3 and A4) sources with $R_{\text{FeII}} \gtrsim 1$ are characterized by the strongest high-ionization outflow, with the largest $\text{CIV}\lambda 1549$ blueshifts (Marziani et al. 2006; Sulentic et al. 2007), and are believed to be the highest Eddington ratio sources. A large low- z sample covering the $\text{H}\beta$ and $\text{MgII}\lambda 2800$ emission lines is defined (§2). We point out intriguing changes of the $\text{H}\beta$ and $\text{MgII}\lambda 2800$ line profile occurring in bins A3 and A4 (§3) and discuss first order considerations

about the physics involved (§4).

2. Sample Selection and Construction of Composite Spectra

We searched SDSS-DR7 for sources catalogued as Type 1 AGN (quasars) in the redshift range $0.4 - 0.75$ and with magnitudes brighter than $g \approx 18.5$ in the g , r or i bands, as well as the Zhou et al. (2006) catalog. The resultant sample consisted of 716 quasars reduced to 680 (all of Pop. B: 369 sources; A1: 97, A2: 156, A3: 43, A4:15) by discarding very noisy spectra and some sources with unusually red colors. Broad Absorption Line (BAL) QSOs were excluded from the sample.

The rest frame was set by measuring the wavelengths of three of the most prominent narrow lines ($[\text{OII}]\lambda 3727$, $\text{H}\beta$, and $[\text{OIII}]\lambda 5007$) when they were detected. Residual systematic wavelength shifts (Hewett & Wild 2010) in addition to the SDSS-provided redshift values were computed taking an average of the three lines in each source spectrum, clipping individual measurements in cases of disagreement because of poor data or intrinsic blueshift of $[\text{OIII}]\lambda 5007$ (Hu et al. 2008). We used IRAF SPLOT to estimate $\text{FWHM}(\text{H}\beta)$ in order to better separate sources into spectral bins following the prescription in Sulentic et al. (2002). Assignments for all bins were made by visual inspection of each spectrum and estimation of R_{FeII} through NGAUSSFIT. Median composites were constructed respectively for $\text{H}\beta$ and $\text{MgII}\lambda 2800$ after redshift correction and continuum normalization at 5050 \AA and 3050 \AA . The rest frame radial velocity of the composites (defined by the average of peak radial velocity of narrow $[\text{OII}]\lambda 3727$, $\text{H}\delta$, $\text{H}\gamma$, $\text{H}\beta$, and $[\text{OIII}]\lambda \lambda 4959, 5007$) was found $< 10 \text{ km s}^{-1}$ in A1 and A2, and $< 20 \text{ km s}^{-1}$ in bin A3 and A4, with a rms value always less than 50 km s^{-1} . A line can be considered unshifted with respect to rest frame if $|\Delta v_r| \leq 100 \text{ km s}^{-1}$. The relative uncertainty of v_r measurements for $\text{H}\beta$ and $\text{MgII}\lambda 2800$ peak velocities on the composite spectra is somewhat less and has been estimated by propagating 3 sources of error on: (1) zero-point; $[\text{OII}]\lambda 3727$ and $\text{H}\beta$ narrow component peak wavelengths measured in the four composites agree within rms $\pm 10 \text{ km s}^{-1}$; (2) wavelength calibration, by measuring the dispersion in wavelength measurements of strong sky lines, typically $\pm 15 \text{ km s}^{-1}$. Systematic shifts are consistent with 0 ($\lesssim 25 \text{ km s}^{-1}$) for $\text{HgI } \lambda 4359$ and $\text{OH } \lambda 8401$ lines whose wavelengths correspond roughly to the wavelengths of the redshifted $\text{MgII}\lambda 2800$ doublet and $\text{H}\beta$ line, respectively; (3) peak line position determined by the multicomponent fit, as provided by the fitting program SPECFIT (§3).

Interpretation of the $\text{H}\beta$ spectral range closely follows previous work (Boroson & Green 1992; Marziani et al. 2003a, 2009). Along with continuum and FeII emission fit over the spectral range $4430 - 5510 \text{ \AA}$, we will include possible contribution of He I lines at 4471

ad 5016 Å (that appear to be significant only for bin A1), HeII λ 4686 and a contribution due to [Fe VII] and [N I] lines at $\approx 5150 - 5200$ Å. The region around MgII λ 2800 has been studied by several authors since the mid-1980s (Wampler 1985; Brotherton et al. 1994; Graham et al. 1996; Laor et al. 1997; Vestergaard & Wilkes 2001). Emission blends near MgII λ 2800 are mainly due to FeII. We define a range for SPECFIT analysis (2600–3050 Å) that is a compromise between proximity to the line and the necessity of having sufficient continuum coverage to properly map the broad FeII blends. We also include other known lines e.g. semi-forbidden Al II] 2669.95 and O III 2672.04. in the fits. Brühweiler & Verner (2008) provide FEII_{UV} emission templates computed from CLOUDY simulations and using an 830 level model of the Fe⁺ ion. Use of the Brühweiler & Verner (2008) FEII_{UV} template results in a systematic residual near 2950 Å (Figs. 1 and 2). The excess flux is probably due to the blend of He II λ 2945 and FeI emission from a cluster of lines produced by transitions from the terms z^5F and a^5D^o to the ground state (a^5D). FeI emission has been predicted by photoionization models (Sigut et al. 2004) and was suggested by previous observations (e.g., Kwan et al. 1995; Graham et al. 1996). The flux deficit is larger than the FeI predicted by photoionization models, at least by a factor of several with respect to a low-ionization, 3 times solar metallicity case (model U20H11 of Sigut et al. 2004). However, several lines associated to FeI multiplets 1 and 9 and opt 30 have been convincingly identified in a strong FeII emitter (Graham et al. 1996), and the emission of Fe I with respect to Fe II might increase with metallicity (Sigut et al. 2004). The issue of Fe I emission deserves further investigation not last because Fe I intensity is strongly dependent on the assumed FeII model at 2900 – 3000 Å. For the sake of present paper we checked that the peak shift of the MgII λ 2800 is basically unaffected even by strong changes in the assumed Fe I strength.

3. Results

3.1. Broad Line Profile Analysis

Composite spectra were analyzed using SPECFIT with χ^2 minimization techniques appropriate for non-linear multi-component fits (Kriss 1994). The procedure allows for simultaneous continuum, FeII and narrow line fitting. Two FEII_{UV} emission templates were applied: the theoretical one by Brühweiler & Verner (2008), and an empirical template produced by Tsuzuki et al. (2006). Use of two independent templates was justified by possible effects that FEII_{UV} subtraction might have on the measurements of line shifts. Continuum subtracted composite spectra are shown in Fig. 1 for bins A1 and A2, and in Fig. 2 and Fig. 3 for bins A3 and A4. The MgII λ 2800 doublet was first modeled as two Lorentzian-like functions of same width and relative intensity ratio 1.25:1. This assumption is justified by the value of

the prototypical A3 source I Zw1, and by the physical conditions within the BLR (Laor et al. 1997). It is possible that the lines become fully thermalized at the extreme optical depth of the low-ionization line (LIL) BLR, justifying the assumption of a 1:1 ratio. We have carried out several fits also for the 1:1 case but the results on line shifts and widths are very close to the 1.25:1 case and do not affect any of the conclusions discussed below.

Table 1 reports the results of the our multi-component analysis: intensity, shift \pm uncertainty at 2σ confidence level (estimated as described at the end of §2), and FWHM of the two line components used to model line profiles: the broad component (BC) and, when appropriate, a blueshifted component (blue). The radial velocity was measured with reference to the vacuum wavelength of the $^2P_{3/2} \rightarrow ^2S_{1/2}$ component, 2796.35 Å. Uncertainties in BC centroid shifts are significantly larger toward the line profile base than at peak, and are estimated to be $\pm 400 \text{ km s}^{-1}$ for the centroid at 1/4 peak intensity. Columns BC and blue Int. report $H\beta$ and $\text{MgII}\lambda 2800$ line intensity normalized by continuum flux at 5050 Å. The normalization at 5050 Å ensures that the $H\beta$ value roughly corresponds to the line equivalent width, and that meaningful intensity ratios $\text{MgII}\lambda 2800/H\beta$ can be computed from the values reported in the Table. Note that $\text{MgII}\lambda 2800$ intensity values are for the doublet, while reported FWHMs are for an individual component. The formal uncertainty in FWHM measurements of $H\beta$ and $\text{MgII}\lambda 2800$ BC is, in absence of systematic effects, around 2% for spectral types A1 and A2, and $\approx 5\%$ in all other cases. Shifts and width of the blue components are subject to considerable larger uncertainties since they are close to the much stronger BC. In addition their values depend on the line profile assumed for the fit. Formal uncertainty (i.e., without considering the possibility of different profile shapes) derived on the FWHM of the blue components is $\lesssim 10\%$ in all cases.

Fits to $H\beta$ and $\text{MgII}\lambda 2800$ in A1 and A2 bins needed only symmetric, unshifted Lorentzian line components. The BC accounts for the entire $H\beta$ and $\text{MgII}\lambda 2800$ profiles in A1 and A2 sources where the ratio $\text{FWHM}(\text{MgII}\lambda 2800) / \text{FWHM}(H\beta) \approx 0.75 - 0.80$ (Tab. 1). This FWHM ratio also holds for Pop. B sources and, therefore, for 90% of quasars (Wang et al. 2009; Trakhtenbrot & Netzer 2012, Sulentic et al. 2012, in preparation). The simplest interpretation is that the emissivity weighted distance of the $\text{MgII}\lambda 2800$ emitting gas is somewhat larger than that for $H\beta$ (≈ 1.5 following the virial assumption, see also §4).

The $H\beta$ profiles in A3 and A4 bins also involve an (almost) unshifted, symmetric component (the broad component BC) with $\text{FWHM}(H\beta_{\text{BC}}) \sim 2000 \text{ km s}^{-1}$ which we assume to be the virial broadening estimator. However, fits to the $H\beta$ profile for sources in A3 and A4 bins require an additional blueshifted (Column “blue” in Tab. 1) component in order to minimize residuals (e.g. Leighly 2000; Leighly & Moore 2004; Marziani et al. 2010; Wang et al. 2011). The “blue” component has been modeled first as a symmetric Gaussian,

in line with past work. The right panels of Fig. 2 show that a good fit to the $\text{MgII}\lambda 2800$ profiles in A3 and A4 is possible using a shifted symmetric Lorentz function with a profile shift of a few hundred km s^{-1} .

At a second stance a skewed Gaussian (Azzalini 1985) has been considered for both $\text{H}\beta$ and $\text{MgII}\lambda 2800$ (Fig. 3). In this case, a two-component model is possible also for the spiky $\text{MgII}\lambda 2800$ profile. We assumed unshifted BC $\text{MgII}\lambda 2800$ emission with $\text{FWHM}(\text{MgII}\lambda 2800) = 0.8 \text{ FWHM}(\text{H}\beta)$, plus an additional blueshifted component described by a skewed Gaussian as for $\text{H}\beta$. The resulting $\text{MgII}\lambda 2800$ line decomposition is shown in the right panels of Fig. 3. Line parameters are reported in Tab. 1 (A3b and A4b).

3.2. A systematic $\text{MgII}\lambda 2800$ Blueshift

Bins A3 and A4 (10% of all quasars) behave differently than the wide majority of quasars since their $\text{FWHM}(\text{MgII}\lambda 2800) \geq \text{H}\beta$. The ratio $\text{FWHM}(\text{MgII}\lambda 2800)/\text{FWHM}(\text{H}\beta)$ is larger than unity in bin A4, with $\text{H}\beta$ and $\text{MgII}\lambda 2800$ showing the same width in bin A3 (lower panel of Fig. 5) where a peak blueshift is already highly significant. As mentioned, the $\text{MgII}\lambda 2800$ doublet appears blueshifted with respect to rest frame and $\text{H}\beta$ in spectral types A3 to A4 where $\text{H}\beta$ shows evidence for a blueshifted component (Fig. 2; see also Marziani et al. 2010). The $\text{MgII}\lambda 2800$ blueshift reaches $\approx 20\%$ of the half line width in bin A4. In bin A3 and A4 the core of the $\text{MgII}\lambda 2800$ profile is narrow enough to appear visually displaced relative to the rest frame (Fig. 2). Even measuring the position of the broad-line core (without any correction because of contaminant lines) with SPLOT we obtain consistent values. The effect is too large to be ascribed to sources of uncertainty on rest frame, and it is even more significant if relative line shifts are considered. As mentioned, we repeated the fits for all bins assuming that the doublet ratio is 1.0:1.0. This results in a slightly larger $\text{MgII}\lambda 2800$ blueshift. To further test the reality of the shift, we considered that the maximum doublet ratio for expected physical conditions in the BLR is 1.5:1.0. We constructed noiseless mock profiles to derive a peak wavelength in case $\text{MgII}\lambda 2800$ treated as single line, for doublet ratios 1.5, 1.25, 1 to 1. The effective wavelength of the doublet is 2799.1, 2799.4, 2800.1 for the three ratios respectively. Also in the case 1.5:1.0, the peak shift will remain significant.

The $\text{MgII}\lambda 2800$ A3 and A4 fits with a shifted symmetric function probably yield only a lower limit to the shift amplitude since, if a two component interpretation is correct, they include also unshifted emission line gas. Yet, these $\text{MgII}\lambda 2800$ fits are meaningful since they provide a robust measurement of a significant blueshift affecting the $\text{MgII}\lambda 2800$ line profile. Renouncing the symmetric Gaussian approximation for the blueshifted emission (in $\text{H}\beta$) provides support for profile decomposition into two components (Fig. 3). With the

exception of A4 $H\beta$, both $H\beta$ and $MgII\lambda 2800$ median spectra show blue components with strong blueward asymmetry: the blue component profiles vaguely resemble the “trapezoidal” shape of the I Zw 1 $CIV\lambda 1549$ profile (c.f. Leighly 2000). The lower v_r derived for $MgII\lambda 2800$ blueshifted component with respect to the one of $H\beta$ in bins A3 and A4 is consistent with the profile shape difference since $H\beta$ is more affected toward the line base, while $MgII\lambda 2800$ is affected to closer to the line core. Indeed, in all cases the shift of $H\beta$ is larger than the shift of $MgII\lambda 2800$. This result provides an important constrain on the emitting region structure (§4). Considering the strongly skewed blue component line profiles in A3 and A4, the estimated shifts reported in Tab.1 could be considered more properly as upper limits since symmetric blueshifted Gaussians would yield some emission under the BC with lower shift values.

The most extreme source in our sample involves SDSS J150813.02+484710.6 whose $MgII\lambda 2800$ and $H\beta$ profiles are shown in Fig. 4. $H\beta$ shows a prominent blue asymmetry while $MgII\lambda 2800$ is fully blueshifted with width and shift amplitude similar to the ones measured for $CIV\lambda 1549$ in extreme Pop. A sources such as I Zw 1. For this source we apply to the $MgII\lambda 2800$ profile only the profile model appropriate for $CIV\lambda 1549$ of extreme Pop. A quasars i.e., an unshifted double Lorentzian + a blueshifted component approximated with a skewed Gaussian. While uncommon, other sources like J1508+48 have been found (see e.g., Q1258+1404; Barthel et al. 1990).

3.3. Major trends

3.3.1. Spectral types

The upper panel of Fig. 5 shows radial velocity v_r trends of broad component peaks as a function of spectral type, while the lower panel shows trends of the ratio $FWHM(MgII\lambda 2800) / FWHM(H\beta)$. $MgII\lambda 2800$ line shift measurements shown in Fig. 5 were carried out in three different ways: (1) using SPECFIT with the theoretical $FEII_{UV}$ template, (2) using SPECFIT with the $FEII_{UV}$ template from Tsuzuki et al. (2006) and (3) measuring the position of the broad-line core without any correction. The three sets of measures yield consistent trends. The interesting change in the lower panel of the figure involves a tendency for the FWHM ratio to increase first to parity in bin A3 and finally to $FWHM(MgII\lambda 2800) > FWHM(H\beta)$ in bin A4 (cf. Trakhtenbrot & Netzer 2012). This trend likely accounts for the large scatter (and convergence toward parity) of single-source measures in Figure 2 of Wang et al. 2009). The consistent behavior of both shift and FWHM strengthens our confidence that the trends are real. The increase in $FWHM(MgII\lambda 2800)$ lends support to the hypothesis that an additional blueshifted component is emerging on the blue side of

an unshifted BC with $\text{FWHM}(\text{MgII}\lambda 2800) \approx 0.8 \text{ FWHM}(\text{H}\beta)$. A symmetric blueshifted Lorentzian model is helpful for ascertaining the reality of the blueshifts but seems physically unrealistic. The blueshifts are more likely associated with a $\text{MgII}\lambda 2800$ component due to gas moving at larger velocity than the ones inferred from the global shift of the line core (Tab. 1).

3.3.2. Eddington ratio

We estimated median M_{BH} values computing median 5100 Å luminosities from fluxes of all sources in each bin and with FWHM measures of the median composites following the prescription of Assef et al. (2011). A bolometric correction to the 5100 Å luminosities was applied following Nemmen & Brotherton (2010) in order to derive L/L_{Edd} values. The semi inter-quartile range (SIQR) of L/L_{Edd} has been estimated using the individual FWHM $\text{H}\beta$ measurements carried out for spectral bin assignment (§2). All bins show very similar median bolometric luminosities $\log L \approx 46.2$ [ergs s⁻¹]. Fig. 6 shows the peak shift of the $\text{MgII}\lambda 2800$ broad and blue components as a function of L/L_{Edd} . Shift values have been normalized by the $\text{H}\beta$ half-width at half-maximum (HW) in order to provide an indicator of dynamical significance to the shifts. The peak $\text{MgII}\lambda 2800$ shift is consistent with zero for spectral types A1 and A2 but begins to appear at $\log L/L_{\text{Edd}} \sim -0.5$ at type A2 increasing to 0.2/0.3 of half width for A3 and A4. The shift amplitude is much larger when the blueshifted component is considered. If $0.8 \cdot \text{HW}$ can be considered as a rough estimator of the virial velocity of the $\text{MgII}\lambda 2800$ emitting gas then A4 and SDSS J1508+4847 show outflows close to escape velocity. The main difference between median A4 and the source SDSS J1508+4847 is related to the amount of outflowing gas: in A4 the blue component is contributing 1/7 of the total line emission while it exceeds 1/3 in SDSS J1508+4847.

4. Discussion

The $\text{MgII}\lambda 2800$ profile in median spectra is different from both $\text{CIV}\lambda 1549$ and $\text{H}\beta$. Comparison between the latter two lines yielded inferences about the BLR structure (Marziani et al. 1996). The $\text{CIV}\lambda 1549$ blueshift in low z sources is thought to be associated with a wind component whose prominence increases with L/L_{Edd} along the 4D eigenvector 1 (4DE1) sequence. The $\text{CIV}\lambda 1549$ profile in bins A2-A4 can be modeled as a combination of the $\text{H}\beta$ BC profile plus a fully blueshifted component that accounts for most of the flux. This basic scenario has been confirmed by recent work (see e.g. Richards et al. 2011; Wang et al. 2011). In the case of $\text{MgII}\lambda 2800$ we see a v_r displacement that is also significant with $200 - 300 \text{ km s}^{-1}$ if

the shift is measured on the full profile. As pointed out, this is likely a lower limit. If the blue component is considered, the shift amplitude is much larger ($\sim -1000 \text{ km s}^{-1}$) but significantly lower in $\text{MgII}\lambda 2800$ than in $\text{H}\beta$. We are considering median spectra so the profiles represent the median behavior of line profiles – in some sense equivalent to a single source rms profile. So we can ask: what is the typical relation between the blueshifted $\text{CIV}\lambda 1549$ and $\text{H}\beta$ on the one hand and the blueshifted $\text{MgII}\lambda 2800$ emission on the other?

4.1. $\text{MgII}\lambda 2800$ blueshift: emission from a radiation-driven wind

The $\text{MgII}\lambda 2800$ blueshift is most straightforwardly interpreted as due to outflow motions of the line emitting gas with preferential obscuration of the receding part of the flow. The fact that large blue shifts are observed when L/L_{Edd} is highest indicates a role of radiation force in acceleration of the gas. If we consider gravitation and ionizing radiation as the only forces (neglecting drag forces and pressure gradients) the radial acceleration can be written as $a(r) \propto \sigma M_{\text{BH}}/r^2 [\alpha(r)/(\sigma N_{\text{c}})L/L_{\text{Edd}} - k]$, where $\alpha(r)$ is the fraction of bolometric luminosity absorbed, N_{c} the column density and σ the Thompson scattering cross-section, and k a constant term. If the first term in square brackets exceeds k , the outflowing velocity field of the gas will follow the form $v(r) = v_{\text{t}}\sqrt{1 - r_{\text{min}}/r}$, where r_{min} is the launching radius of the wind, and v_{t} the terminal velocity ($\propto \sqrt{L/r_{\text{min}}}$). Outflows driven by line and/or ionizing photon pressure can accelerate the line-emitting gas to $v_{\text{t}} \approx k'(\mathcal{M}L/r)^{\frac{1}{2}} \approx (\mathcal{M}L/L_{\text{Edd}})^{\frac{1}{2}} v_{\text{Kepl}}$ where v_{Kepl} is the Keplerian velocity at the launching radius of the wind (e.g. Laor & Brandt 2002). In the case of outflows driven by ionizing radiation the force multiplier \mathcal{M} is expected to be: $\mathcal{M} = \frac{\alpha}{\sigma N_{\text{c}}} \approx 7.5\alpha_{0.5}N_{\text{c},23}^{-1}$ where $\alpha \approx 0.5$ for Compton-thin gas optically thick to the ionizing continuum (Netzer & Marziani 2010). \mathcal{M} can be $\gg 1$ in the case of line driven winds (Proga et al. 2000).

The largest $\text{CIV}\lambda 1549$ blue shifts are observed in spectral types A3 and A4 (in A3, $-1000 \lesssim \Delta v_{\text{r}} \lesssim -2000 \text{ km s}^{-1}$) where also the $\text{MgII}\lambda 2800$ shifts occur. It therefore seems unlikely that there is no connection between $\text{CIV}\lambda 1549$ and $\text{MgII}\lambda 2800$: both lines may be emitted as part of the same flow. However, bulk emission are expected to occur at different distances and/or in different physical condition. In the framework of photoionization, $\text{MgII}\lambda 2800$ emission is associated with low-ionization and relatively large column density gas (Netzer 1980; Korista et al. 1997). Within a gas slab or cloud, $\text{MgII}\lambda 2800$ is emitted mainly beyond the fully ionized zone of geometrical depth $h \sim 10^{23}U n_{\text{H}}^{-1}$ (with U being the ionization parameter) where all of the $\text{CIV}\lambda 1549$ is emitted. The total column density needed for substantial $\text{MgII}\lambda 2800$ production is not well constrained at very low ionization, since the fully ionized zone is already a tiny fraction of the emitting gas slab if $N_{\text{c}} \sim 10^{23}$.

cm^{-2} and $\log U \lesssim -1$.

Since v_t is proportional to both $N_c^{-1/2}$ and $r_{\min}^{-1/2}$, MgII λ 2800 emission may occur at higher column density and/or larger distance than blueshifted CIV λ 1549. A large r_{\min} is consistent with the overall symmetry of the MgII λ 2800 profile base (§3.2; Figs. 1, 2, 3). Reverberation mapping indicates that high ionization lines are emitted closer to the central continuum than low-ionization lines (e.g. Peterson & Wandel 1999). It is possible to ascribe the blueshifted MgII λ 2800 emission entirely to a larger radial distance if MgII λ 2800 arises ~ 2 times more distant than CIV λ 1549. On the other hand, if $L/L_{\text{Edd}} \rightarrow 1$, $v_t \approx \sqrt{\mathcal{M}}v_{\text{vir}}$. Restricting our considerations to order-of-magnitude estimates due to uncertain shift values, a reasonable increase in column density over the standard value $N_c \sim 10^{23} \text{ cm}^{-2}$ would also suffice to reduce the MgII λ 2800 shifts close to the observed values.

An assumption from the behavior of the FWHM ratio is that the MgII λ 2800 flows start close to where the bulk of the low-ionization lines (H β in the present case) is emitted. The following considerations apply also if $\text{FWHM}(\text{MgII}\lambda 2800)/\text{FWHM}(\text{H}\beta) \approx 0.8$ implies $\approx 1.5 \times$ larger emissivity-weighted distance for MgII λ 2800 than for H β . The distance from the continuum source of the emitting gas r_{em} can be derived from the continuum luminosity at 5100 Å following Bentz et al. (2009): $\log r_{\text{em}} \approx 17.6$ [cm] for spectral type A4. If $\log n_{\text{H}} = 12$ [cm^{-3}], the ionization parameter is $\log U \approx -2.8$. The MgII λ 2800 luminosity is then $L(\text{MgII}\lambda 2800) = 4\pi r_{\text{em}}^2 f_c \sigma_{\text{em}} = 4\pi r_{\text{em}}^2 f_c \bar{\epsilon} \frac{N_c}{n_{\text{H}}}$, where f_c is the covering factor, σ_{em} the emerging line flux for unit surface, and $\bar{\epsilon}$ the depth-averaged volume emissivity. CLOUDY (Ferland et al. 1998) simulations indicate that σ_{em} has a minimum value $\approx 10^{7.8} \text{ ergs s}^{-1} \text{ cm}^{-2}$ at $\log n_{\text{H}} = 12$ if $-2.8 \lesssim \log U \lesssim -2$, $10^{23} \text{ cm}^{-2} \lesssim N_c \lesssim 10^{25} \text{ cm}^{-2}$, $12 \leq \log n_{\text{H}} \leq 13$. In these ranges σ_{em} depends slightly on N_c and U . The computed $L(\text{MgII}\lambda 2800)$ extrapolated to full continuum coverage is always larger than the observed $L(\text{MgII}\lambda 2800)$ ($\approx 10^{43.5} \text{ ergs s}^{-1}$ for A4). This is the case if the geometry is assumed static and open or if a velocity field appropriate for a wind (i.e., with photon local escape probability following Sobolev’s approximation) is considered. The derived $f_c \lesssim 0.2$ indicates partial covering of the continuum as in a wind or in an ensemble of outflowing clouds.

Resonant line acceleration is expected to contribute to the dynamics of the flow in the physical scenario outlined above. Circumstantial evidence in favor of line acceleration is provided by the difference between a resonance UV line (MgII λ 2800) and a non-resonance line (H β). From the purely observational point of view, a line driven outflow would be convincingly demonstrated if the ionizing photon flux were found unable to drive the line emitting gas to the observed outflow velocity or, in the context of absorption lines, from “line locking” (e.g. Cottis et al. 2010). However, the ionizing photon flux appears to be sufficient to accelerate the gas to the observed MgII λ 2800 velocities and to escape velocity

in A4 sources: for $\log L/L_{\text{Edd}} \approx -0.2$, $\mathcal{M} \approx 7.5$, $v_t \approx 1.8v_{\text{Kepl}}$. If $v_{\text{Kepl}} \approx 0.8\text{HW}(\text{H}\beta)$, $v_t \approx 1500 \text{ km s}^{-1}$. This value exceeds the peak velocity of the blue component in bin A3, and is in agreement with the ones measured in A4 and in SDSS J1508+4847. Resonant line acceleration might be needed if the gas has a large N_c ($\gtrsim 10^{23} \text{ cm}^{-2}$) or if the $\text{MgII}\lambda 2800$ emitting gas is shielded by part of the continuum.

4.2. Alternate interpretations

Both $\text{MgII}\lambda 2800$ and $\text{H}\beta$ line profile widths are probably modified by the viewing angle of the outflow/jet axis. Evidence exists that the line width of $\text{H}\beta$ is affected by line-of-sight orientation of the jet axis in radio-loud sources (Wills & Browne 1986; Wills & Brotherton 1995; Rokaki et al. 2003; Sulentic et al. 2003; Zamfir et al. 2008). An effect on FWHM of a factor ≈ 2 is likely between core and lobe-dominated sources. Orientation effects are also expected for radio-quiet quasars (e.g. Jarvis & McLure 2006; Punsly & Zhang 2010). Extreme and variable soft X-ray emission from some narrow line Seyfert 1s (Pop. A) sources has been interpreted as a signature of pole-on orientation (Sulentic et al. 2000, and references therein). Recent work confirms a dependence on orientation for $\text{H}\beta$ in radio-loud sources and further suggests a less-strong dependence for $\text{MgII}\lambda 2800$ (Runnoe et al. 2012). Following this line of reasoning the occurrence of blueshifts in bin A3/A4 might involve sources viewed at a favorable line-of-sight orientation. It is not clear whether the results of Runnoe et al. (2012) on different orientation sensitivity can be extended to Pop. A where radio-loud sources are almost absent in bins A2, A3 and A4. Even if the $\text{FWHM}(\text{H}\beta)$ change could be explained on the basis of an orientation effect, several line intensity ratios change very strongly going from A1 to A4 (e.g., Wills et al. 1999; Aoki & Yoshida 1999; Sulentic et al. 2000; Bachev et al. 2004; Baldwin et al. 2004; Negrete et al. 2012; Shin et al. 2012): R_{FeII} by definition, but also $\text{CIII}] \lambda 1909 / \text{SiIII}] \lambda 1892$, $\text{AlIII} \lambda 1860 / \text{SiIII}] \lambda 1892$, $\text{SiIV} \lambda 1397 + \text{OIV}] \lambda 1402 / \text{CIV} \lambda 1549$. Emission line equivalent widths change as well. For instance, the EW of $\text{H}\beta$ BC shows a decrease from A1 to A4 by a factor ≈ 2 (Tab. 1), as found previously (e.g., Sulentic et al. 2000). The large difference in EW persists also if the flux of the blueshifted component is included. Line intensity ratios and line equivalent widths are most likely sensitive to density, ionization state and chemical composition of the gas along with ionizing continuum shape (ultimately thought to be governed by Eddington ratio). In this respect we note that the decrease of $W(\text{MgII}\lambda 2800)$ from ≈ 110 to $\approx 70 \text{ \AA}$ is also consistent with a study showing an anticorrelation between $W(\text{MgII}\lambda 2800)$ and L/L_{Edd} (Dong et al. 2009). It is unclear how orientation might drive such changes. We are probably dealing with a restricted range of L/L_{Edd} in each spectral bin “convolved” with the effect of orientation (Marziani et al. 2001). If a (rare) pole-on orientation favors the observation of large shifts then SDSS J1508+4847 might be

an example of a pole-on source.

5. Conclusion

MgII λ 2800 should be used as a virial estimator with caution in high Eddington ratio sources. Under the simplest assumptions virial motion implies an unshifted and symmetric profile. A systematic line profile blueshift can be interpreted as the signature of emission from radiatively acceleration of gas motion therefore invalidating the virial broadening assumption for MgII λ 2800 in 20% of Pop. A sources (10% of all quasars). Conversely further work has shown that the majority of quasars show unshifted MgII λ 2800 profiles that are more symmetric than H β (Sulentic et al. 2012 in preparation, and references therein). The width of MgII λ 2800 is probably a suitable virial broadening estimator for those sources.

PM acknowledges Junta de Andalucía, through grant TIC-114 and the Excellence Project P08-TIC-3531, and the Spanish Ministry for Science and Innovation through grants AYA2010-15169 for supporting a sabbatical stay at IAA-CSIC. I. P. - F. acknowledges the postdoctoral fellowship grants 145727 and 170304 from CONACyT Mexico. The authors wish to thank an anonymous referee whose suggestions helped them to critically reanalyze some of their results. Funding for the SDSS and SDSS-II has been provided by the Alfred P. Sloan Foundation, the Participating Institutions, the National Science Foundation, the U.S. Department of Energy, the National Aeronautics and Space Administration, the Japanese Monbukagakusho, the Max Planck Society, and the Higher Education Funding Council for England. The SDSS Web Site is <http://www.sdss.org/>. Full acknowledgement of SDSS is given at <http://www.sdss.org/collaboration/credits.html>.

Table 1: Derived Quantities from the $H\beta$ and $MgII\lambda 2800$ Profile Multicomponent Analysis

Sp. T.	$H\beta$						$MgII\lambda 2800$					
	BC			blue			BC			blue		
	Int. ^a	Shift ^b	FWHM ^b	Int. ^a	Shift ^b	FWHM ^b	Int. ^c	Shift ^b	FWHM ^b	Int. ^c	Shift ^b	FWHM ^b
A1	96	20 \pm 40	3180	0.0	n.a.	n.a.	111	35 \pm 50	2710	0.0	n.a.	n.a.
A2	85	-20 \pm 40	2900	0.0	n.a.	n.a.	73	-70 \pm 50	2320	0.0	n.a.	n.a.
A3	45	45 \pm 40	2190	12	-1240 \pm 230	4250	65	-150 \pm 50	2240	0.0	n.a.	n.a.
A3b	54	45 \pm 40	2190	6.5	-1420 \pm 510	4100	54	0 ^d	1750 ^e	5.6	-880 \pm 170	3100
A4	28	70 \pm 50	1980	16	-1240 \pm 220	4870	68	-265 \pm 90	2650	0.0	n.a.	n.a.
A4b	29	70 \pm 50	1940	13	-1530 \pm 200	4460	46	0 ^d	1585 ^e	10	-1010 \pm 130	3300
J1508+48	32	-5 ^d	2300	5.0	-1540 \pm 100	4000	37	0 ^d	2190	20	-1490 \pm 160	3500

^a Line intensity normalized to the continuum at 5050 Å. The value roughly corresponds to the rest-frame equivalent width in Å. For J1508+48 values are in units of 10^{-15} ergs s^{-1} cm^{-2} Å $^{-1}$.

^b In units of km s^{-1} .

^c Line intensity normalized to the continuum at 5050 Å. The value can be used an estimate of the $MgII\lambda 2800/H\beta$ intensity ratio. For J1508+48 values are in units of 10^{-15} ergs s^{-1} cm^{-2} Å $^{-1}$.

^d Imposed to be consistent with rest frame.

^e $FWHM(MgII\lambda 2800) = 0.8 FWHM(H\beta)$, for broad component.

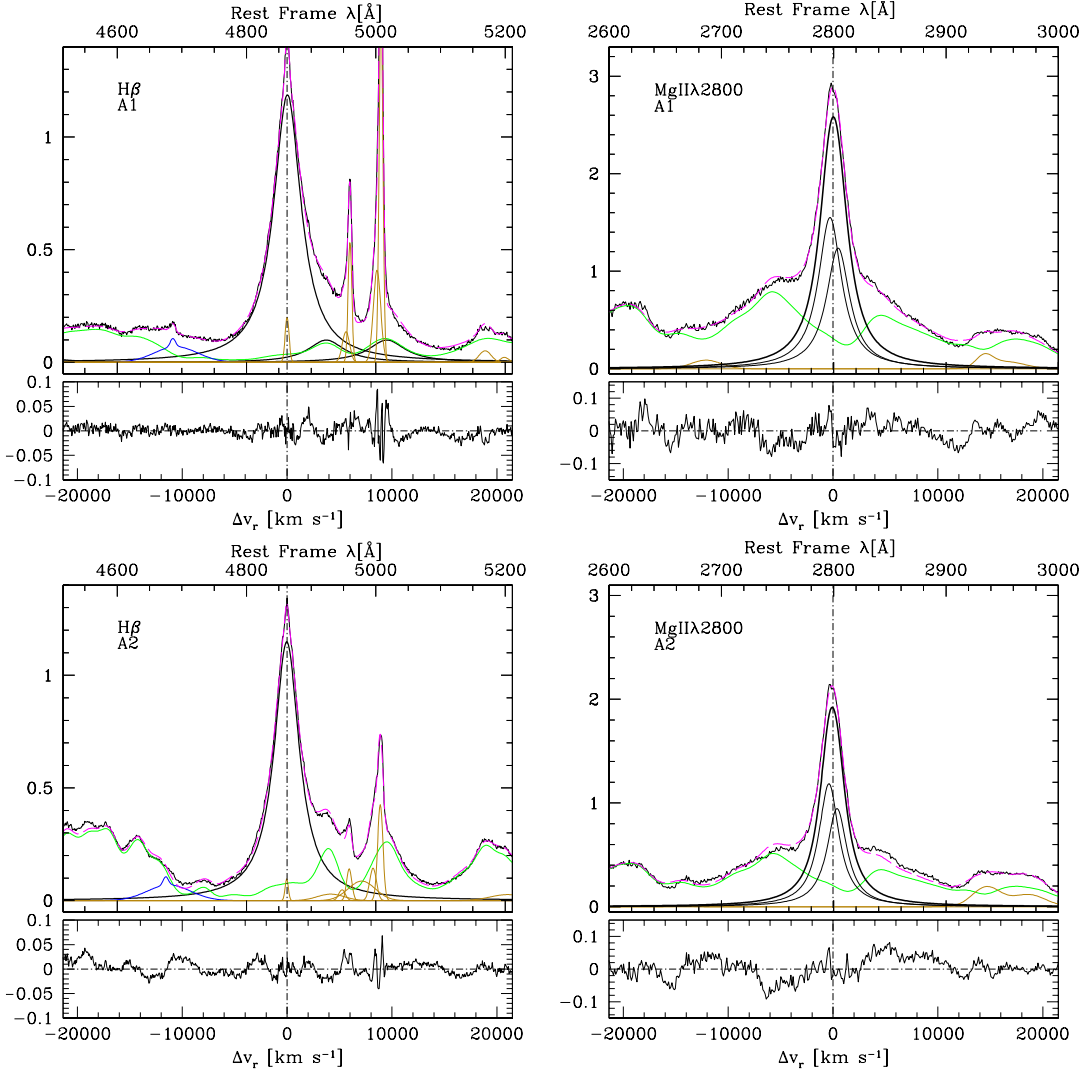


Fig. 1.— Spectra of $H\beta$ (left panels) and $MgII\lambda 2800$ (right panels) for spectral types A1 (top) and A2 (bottom). The horizontal scale is rest frame wavelength [\AA] or radial velocity with the origin indicating rest frame (laboratory) wavelength. In the $MgII\lambda 2800$ panels the vertical dot-dashed line is drawn at the reference wavelength 2799.4 which corresponds to a component ratio 1.25:1.00. The black lines show the original continuum-subtracted spectrum while the dashed magenta line shows the model including all emission line components. The thick black lines show the broad component and thin black lines the individual components of the $MgII\lambda 2800$ doublet. The green lines trace $Fe II_{opt}$ and $Fe II_{UV}$ emission and the gold-brown lines various contributions associated with the narrow-line region ($H\beta_{NC}$, $[OIII]\lambda\lambda 4959, 5007$). In the $H\beta$ panels significant $He II\lambda 4686$ is revealed (thick blue line). In the A1 $H\beta$ panel $He II\lambda 4924$ and $He II\lambda 5016$ (black lines) almost overlap with the m42 $Fe II_{opt}$ lines. The $Fe I + He II\lambda 2945$ emission (modeled as the sum of two Gaussians) is also traced by a brown line and is visible toward the right end of the $MgII\lambda 2800$ panel at $\approx 2950\text{\AA}$.

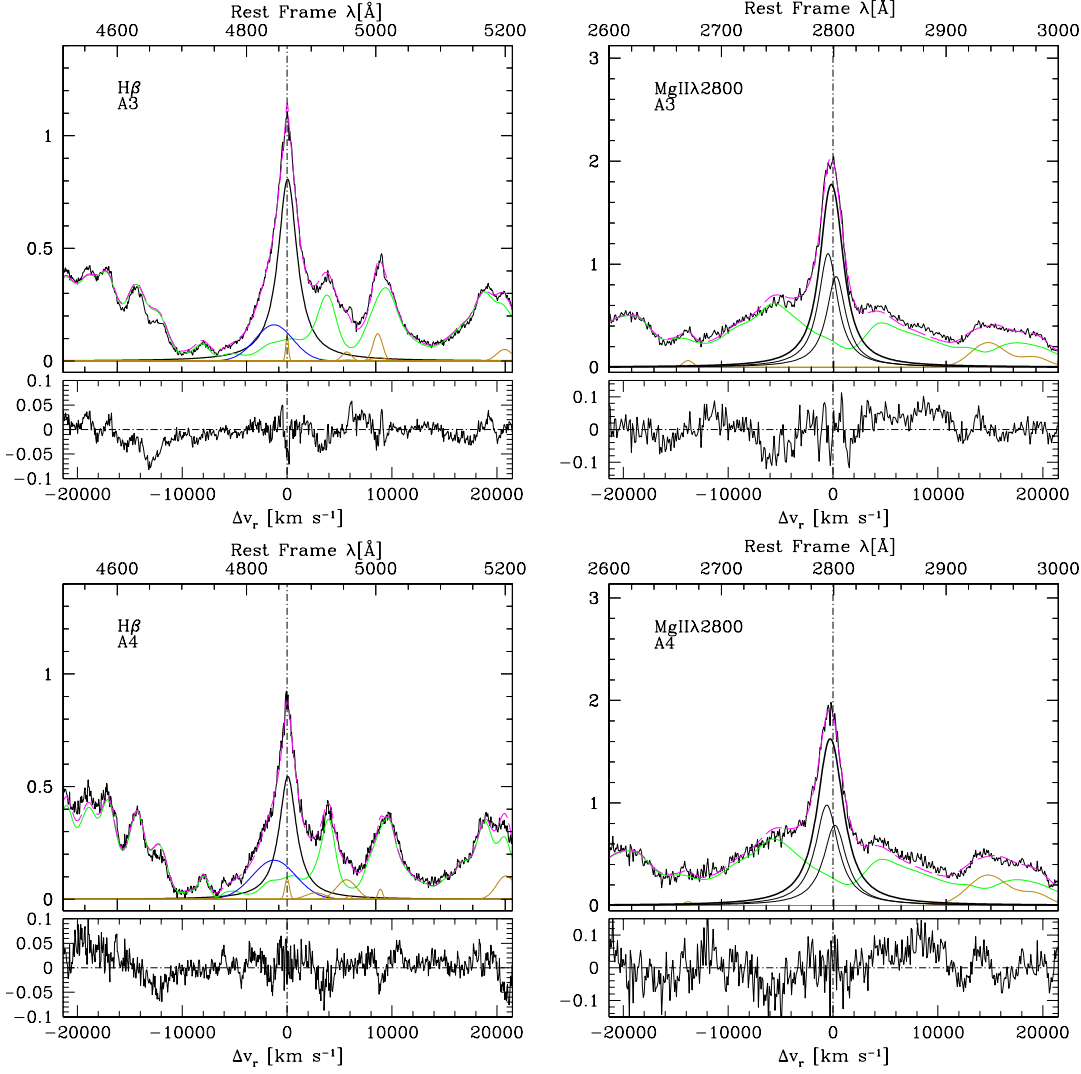


Fig. 2.— Spectra of $H\beta$ (left panels) and $MgII\lambda 2800$ (right panels) for spectral types A3 (top) and A4 (bottom). The right panels show a model that assumes a shifted BC for $MgII\lambda 2800$ and an almost unshifted BC + a blueshifted Gaussian component (thick blue line) for $H\beta$. Meaning of all other symbols is the same as Figure 1.

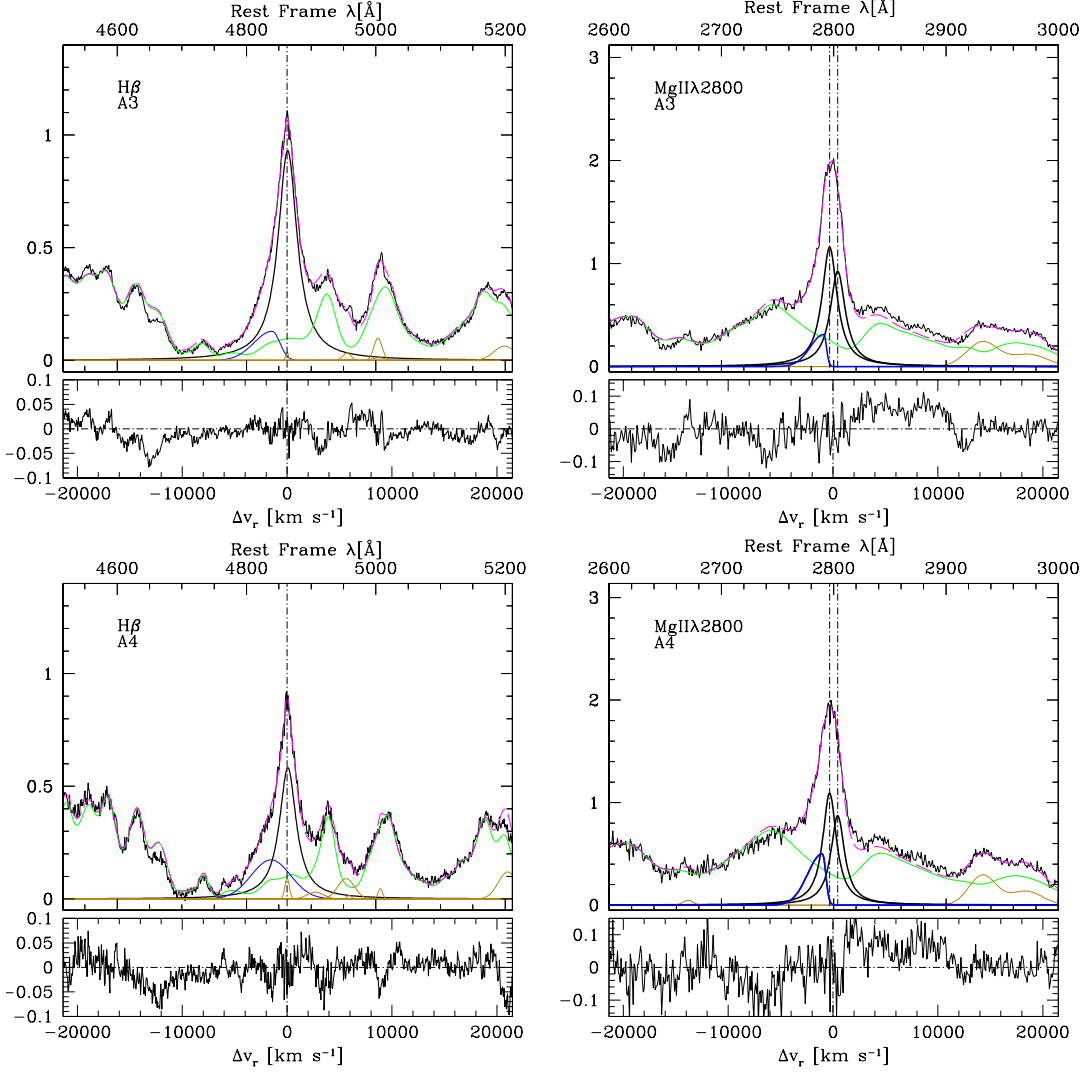


Fig. 3.— Spectra of H β (left panels) and MgII λ 2800 (right panels) for spectral types A3 (top) and A4 (bottom), as in the previous figure. The panels show models of both H β (left) and MgII λ 2800 that assume an (almost) unshifted BC and a blueshifted skewed Gaussian component. Meaning of symbols is the same as Fig. 2 except for the individual MgII λ 2800 components that are shown by thick lines in the right panels. Reference dot-dashed lines are drawn at the vacuum laboratory wavelength of the two MgII λ 2800 components.

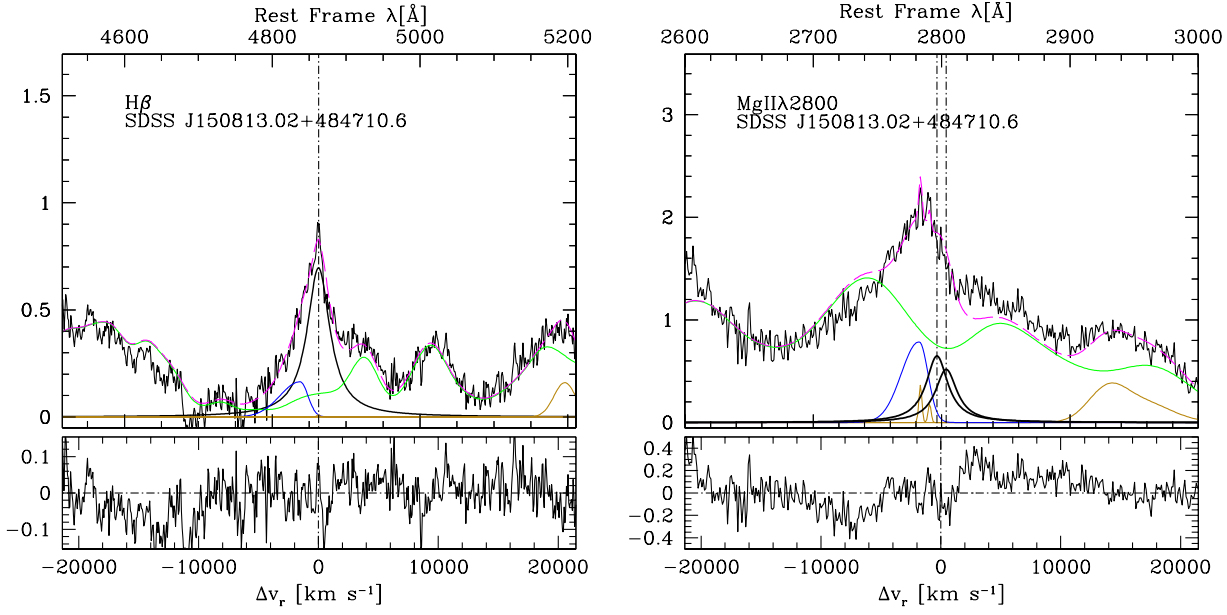


Fig. 4.— Spectra of H β (left panels) and MgII λ 2800 (right panels) for quasar SDSS J150813.02+484710.6. Vertical scale is specific flux in units of 10^{-15} ergs s $^{-1}$ cm $^{-2}$ Å $^{-1}$. The meaning of all other symbols is the same as Figs. 1 and 3.

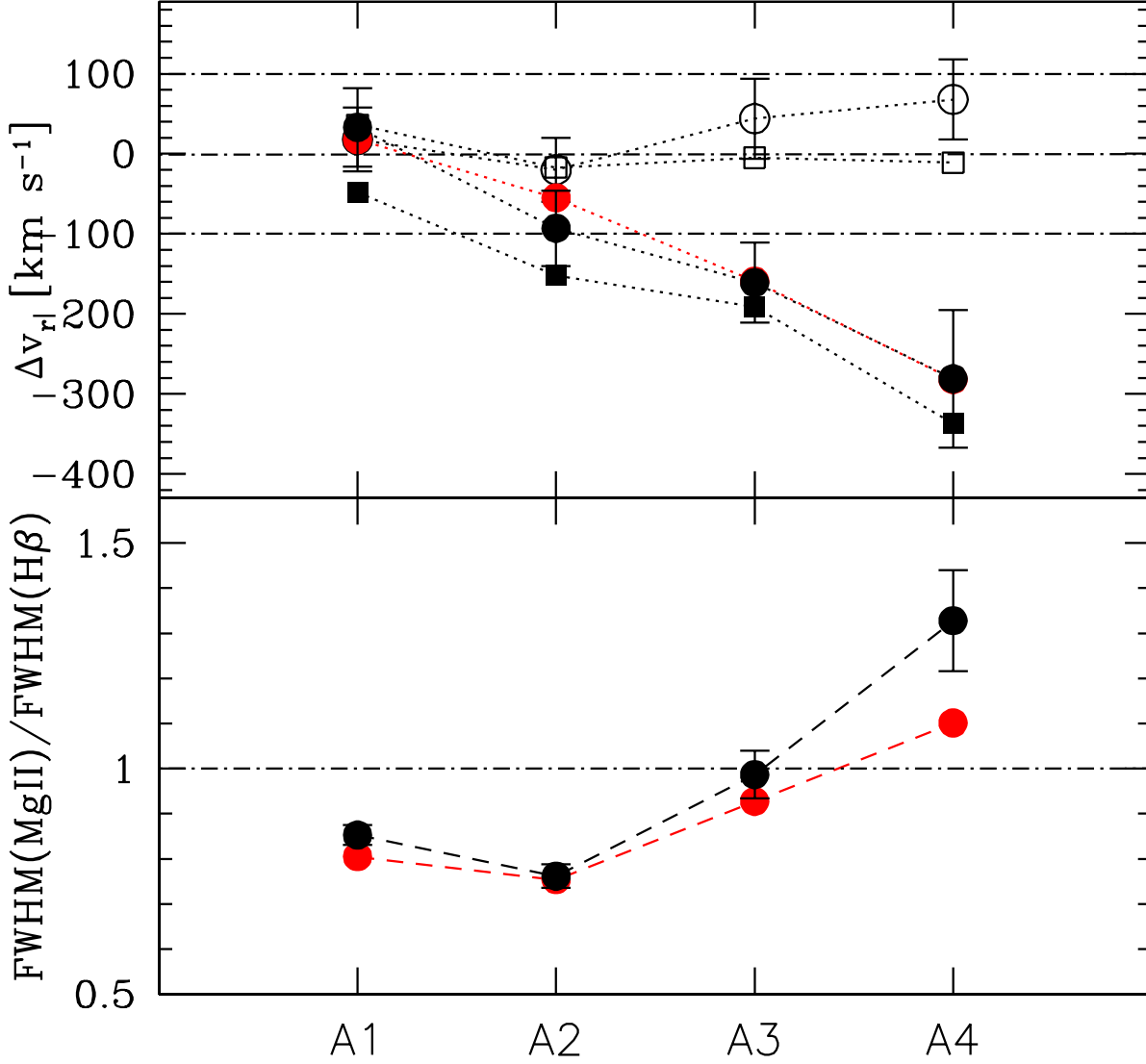


Fig. 5.— Trends in Pop. A as a function of spectral type. Filled circles: MgII λ 2800; open circles: H β . In the upper panel the BC shifts are relative to rest frame. Error bars are at 2σ confidence level, and are shown only for one measure of H β and one of MgII λ 2800 for clarity. The squares indicate an additional measurement of the core centroid of the line obtained after removal of NC emission. The red circles refer to measurements obtained applying the FeII template of Tsuzuki et al. (2006) in the region of MgII λ 2800. The dot dashed lines at ± 100 km s $^{-1}$ in the top panel defines a zone where peak measurements are consistent with zero shift (at 2σ confidence level). In the lower panel the ratio FWHM(MgII λ 2800) (individual component) over FWHM(H β_{BC}) is plotted. Error bars are again at 2σ confidence level.

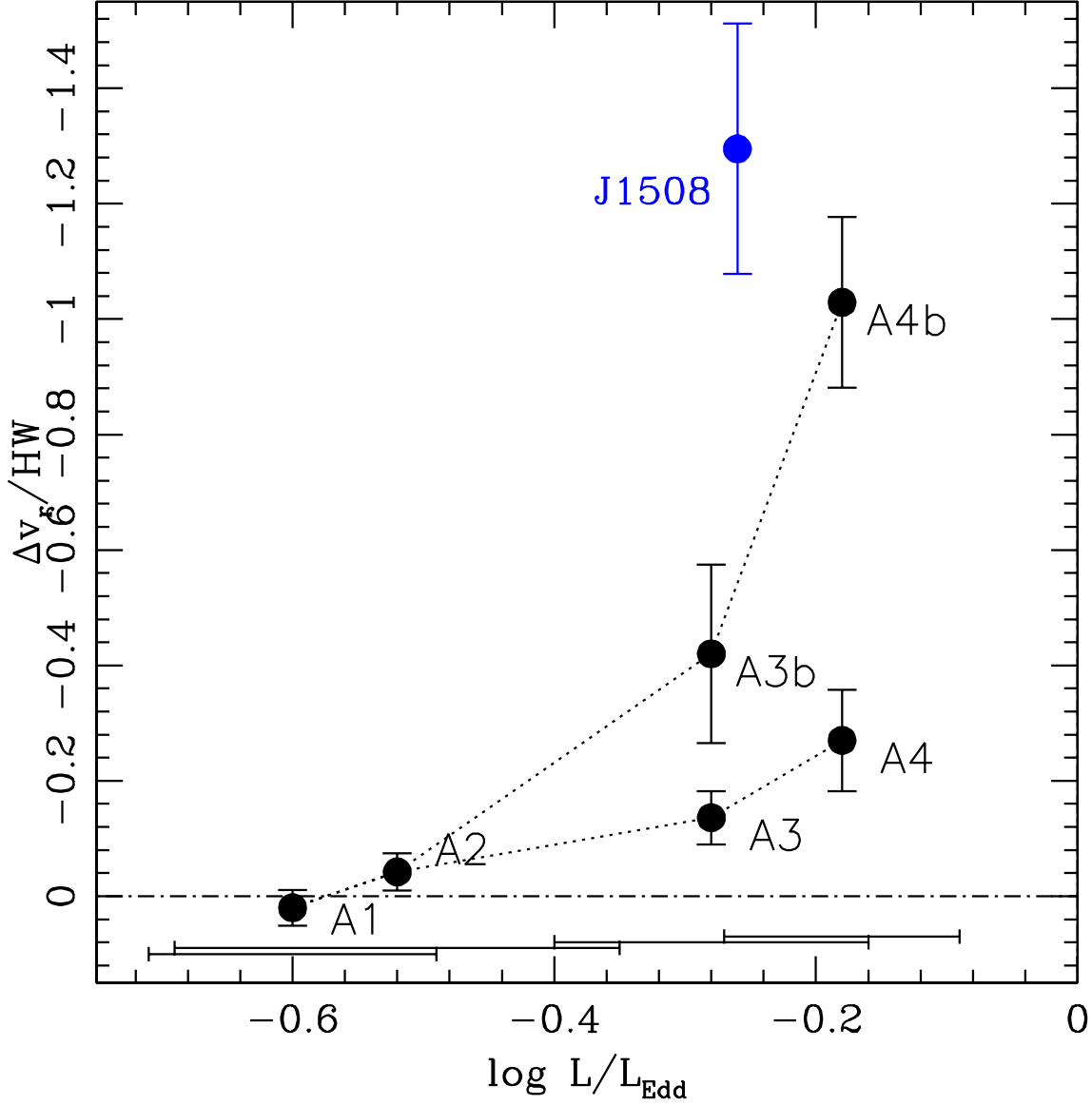


Fig. 6.— The ratio between the peak $\text{MgII}\lambda 2800$ shift and $\text{H}\beta$ half-width half maximum (HWHM) as a function of Eddington ratio. Data points are shown for an unresolved $\text{MgII}\lambda 2800$ fit (A1, A2, A3, A4), as well as for the blueshifted component in two component fits (A3b and A4b). Error bars are at 2σ confidence level. SIQRs in L/L_{Edd} values are ≈ 0.1 for bins A1, A3, A4, and ≈ 0.16 in bin A2. Eddington ratio ranges corresponding to $\pm \text{SIQR}$ are indicated in the lower part of the diagram for all four spectral types. The blue data point refers to a two component fit for source SDSS J150813.02+484710.6.

REFERENCES

- Aoki, K., & Yoshida, M. 1999, in *Astronomical Society of the Pacific Conference Series*, Vol. 162, *Quasars and Cosmology*, ed. G. Ferland & J. Baldwin, 385
- Assef, R. J., et al. 2011, *ApJ*, 742, 93
- Azzalini, A. 1985, *Scand. J. Statist.*, 12, 171
- Bachev, R., Marziani, P., Sulentic, J. W., Zamanov, R., Calvani, M., & Dultzin-Hacyan, D. 2004, *ApJ*, 617, 171
- Baldwin, J. A., Ferland, G. J., Korista, K. T., Hamann, F., & LaCluyzé, A. 2004, *ApJ*, 615, 610
- Barthel, P. D., Tytler, D. R., & Thomson, B. 1990, *A&ApS*, 82, 339
- Bentz, M. C., Peterson, B. M., Pogge, R. W., & Vestergaard, M. 2009, *ApJL*, 694, L166
- Boroson, T. A. 2002, *ApJ*, 565, 78
- Boroson, T. A., & Green, R. F. 1992, *ApJS*, 80, 109
- Bottorff, M., Korista, K. T., Shlosman, I., & Blandford, R. D. 1997, *ApJ*, 479, 200
- Brotherton, M. S., Wills, B. J., Steidel, C. C., & Sargent, W. L. W. 1994, *ApJ*, 423, 131
- Brühweiler, F., & Verner, E. 2008, *ApJ*, 675, 83
- Collin, S., Kawaguchi, T., Peterson, B. M., & Vestergaard, M. 2006, *A&Ap*, 456, 75
- Cottis, C. E., Goad, M. R., Knigge, C., & Scaringi, S. 2010, *MNRAS*, 406, 2094
- Denney, K. D. 2012, *ApJ*, 759, 44
- Dong, X.-B., Wang, T.-G., Wang, J.-G., Fan, X., Wang, H., Zhou, H., & Yuan, W. 2009, *ApJ*, 703, L1
- Ferland, G. J., Korista, K. T., Verner, D. A., Ferguson, J. W., Kingdon, J. B., & Verner, E. M. 1998, *PASP*, 110, 761
- Gaskell, C. M. 1982, *ApJ*, 263, 79
- Graham, M. J., Clowes, R. G., & Campusano, L. E. 1996, *MNRAS*, 279, 1349
- Grupe, D. 2004, *AJ*, 127, 1799

- Hewett, P. C., & Wild, V. 2010, MNRAS, 405, 2302
- Hu, C., Wang, J.-M., Ho, L. C., Chen, Y.-M., Zhang, H.-T., Bian, W.-H., & Xue, S.-J. 2008, ApJ, 687, 78
- Jarvis, M. J., & McLure, R. J. 2006, MNRAS, 369, 182
- Korista, K., Baldwin, J., Ferland, G., & Verner, D. 1997, ApJS, 108, 401
- Kriss, G. 1994, Astronomical Data Analysis Software and Systems III, A.S.P. Conference Series, 61, 437
- Kruczek, N. E., et al. 2011, AJ, 142, 130
- Kwan, J., Cheng, F.-Z., Fang, L.-Z., Zheng, W., & Ge, J. 1995, ApJ, 440, 628
- Laor, A., & Brandt, W. N. 2002, ApJ, 569, 641
- Laor, A., Jannuzi, B. T., Green, R. F., & Boroson, T. A. 1997, ApJ, 489, 656
- Leighly, K. M. 2000, NARev, 44, 395
- Leighly, K. M., & Moore, J. R. 2004, ApJ, 611, 107
- Marziani, P., Dultzin-Hacyan, D., & Sulentic, J. W. 2006, Accretion onto Supermassive Black Holes in Quasars: Learning from Optical/UV Observations (New Developments in Black Hole Research), 123
- Marziani, P., & Sulentic, J. W. 2012, NARev, 56, 49
- Marziani, P., Sulentic, J. W., Dultzin-Hacyan, D., Calvani, M., & Moles, M. 1996, ApJS, 104, 37
- Marziani, P., Sulentic, J. W., Negrete, C. A., Dultzin, D., Zamfir, S., & Bachev, R. 2010, MNRAS, 409, 1033
- Marziani, P., Sulentic, J. W., Stirpe, G. M., Zamfir, S., & Calvani, M. 2009, A&Ap, 495, 83
- Marziani, P., Sulentic, J. W., Zamanov, R., Calvani, M., Dultzin-Hacyan, D., Bachev, R., & Zwitter, T. 2003a, ApJS, 145, 199
- Marziani, P., Sulentic, J. W., Zwitter, T., Dultzin-Hacyan, D., & Calvani, M. 2001, ApJ, 558, 553
- Marziani, P., Zamanov, R. K., Sulentic, J. W., & Calvani, M. 2003b, MNRAS, 345, 1133

- Murray, N., & Chiang, J. 1997, *ApJ*, 474, 91
- Negrete, A., Dultzin, D., Marziani, P., & Sulentic, J. 2012, *ApJ*, 757, 62
- Nemmen, R. S., & Brotherton, M. S. 2010, *MNRAS*, 408, 1598
- Netzer, H. 1980, *ApJ*, 236, 406
- Netzer, H., Lira, P., Trakhtenbrot, B., Shemmer, O., & Cury, I. 2007, *ApJ*, 671, 1256
- Netzer, H., & Marziani, P. 2010, *ApJ*, 724, 318
- Peterson, B. M., & Wandel, A. 1999, *ApJ*, 521, L95
- Proga, D., Stone, J. M., & Kallman, T. R. 2000, *ApJ*, 543, 686
- Punsly, B., & Zhang, S. 2010, *ApJ*, 725, 1928
- Richards, G. T., et al. 2011, *AJ*, 141, 167
- Rokaki, E., Lawrence, A., Economou, F., & Mastichiadis, A. 2003, *MNRAS*, 340, 1298
- Runnoe, J. C., Brotherton, M., Shang, Z., Wills, B., & DiPompeo, M. 2012, *ArXiv e-prints*
- Shin, J., Woo, J.-H., Nagao, T., & C., K. S. 2012, *ApJ*, in press
- Sigut, T. A. A., Pradhan, A. K., & Nahar, S. N. 2004, *ApJ*, 611, 81
- Sulentic, J. W., Bachev, R., Marziani, P., Negrete, C. A., & Dultzin, D. 2007, *ApJ*, 666, 757
- Sulentic, J. W., Marziani, P., & Dultzin-Hacyan, D. 2000, *ARA&A*, 38, 521
- Sulentic, J. W., Marziani, P., Zamanov, R., Bachev, R., Calvani, M., & Dultzin-Hacyan, D. 2002, *ApJL*, 566, L71
- Sulentic, J. W., Zamfir, S., Marziani, P., Bachev, R., Calvani, M., & Dultzin-Hacyan, D. 2003, *ApJL*, 597, L17
- Tang, B., Shang, Z., Gu, Q., Brotherton, M. S., & Runnoe, J. C. 2012, *ApJS*, 201, 38
- Trakhtenbrot, B., & Netzer, H. 2012, *ArXiv e-prints*
- Tsuzuki, Y., Kawara, K., Yoshii, Y., Oyabu, S., Tanabé, T., & Matsuoka, Y. 2006, *ApJ*, 650, 57
- Tytler, D., & Fan, X.-M. 1992, *ApJS*, 79, 1

- Véron-Cetty, M.-P., Véron, P., & Gonçalves, A. C. 2001, *AAp*, 372, 730
- Vestergaard, M., & Wilkes, B. J. 2001, *ApJS*, 134, 1
- Wampler, E. J. 1985, *ApJ*, 296, 416
- Wang, H., Wang, T., Zhou, H., Liu, B., Wang, J., Yuan, W., & Dong, X. 2011, *ApJ*, 738, 85
- Wang, J., et al. 2009, *ApJ*, 707, 1334
- Wills, B. J., & Brotherton, M. S. 1995, *ApJ*, 448, L81
- Wills, B. J., & Browne, I. W. A. 1986, *ApJ*, 302, 56
- Wills, B. J., Laor, A., Brotherton, M. S., Wills, D., Wilkes, B. J., Ferland, G. J., & Shang, Z. 1999, *ApJ*, 515, L53
- Zamfir, S., Sulentic, J. W., & Marziani, P. 2008, *MNRAS*, 387, 856
- Zhou, H., Wang, T., Yuan, W., Lu, H., Dong, X., Wang, J., & Lu, Y. 2006, *ApJS*, 166, 128